



Evidence that 1I/2017 U1 (‘Oumuamua) was Composed of Molecular Hydrogen Ice

Darryl Seligman¹ and Gregory Laughlin² ¹Dept. of the Geophysical Sciences, University of Chicago, Chicago, IL 60637, USA; dzseligman@uchicago.edu²Dept. of Astronomy, Yale University, New Haven, CT 06517, USA

Received 2020 April 13; revised 2020 May 24; accepted 2020 May 26; published 2020 June 9

Abstract

‘Oumuamua (1I/2017 U1) was the first macroscopic ($l \sim 100$ m) body observed to traverse the inner solar system on an unbound hyperbolic orbit. Its light curve displayed strong periodic variation, and it showed no hint of a coma or emission from molecular outgassing. Astrometric measurements indicate that ‘Oumuamua experienced nongravitational acceleration on its outbound trajectory, but energy balance arguments indicate this acceleration is inconsistent with a water ice sublimation-driven jet of the type exhibited by solar system comets. We show that all of ‘Oumuamua’s observed properties can be explained if it contained a significant fraction of molecular hydrogen (H_2) ice. H_2 sublimation at a rate proportional to the incident solar flux generates a surface-covering jet that reproduces the observed acceleration. Mass wasting from sublimation leads to monotonic increase in the body axis ratio, explaining ‘Oumuamua’s shape. Back-tracing ‘Oumuamua’s trajectory through the solar system permits calculation of its mass and aspect ratio prior to encountering the Sun. We show that H_2 -rich bodies plausibly form in the coldest dense cores of giant molecular clouds, where number densities are of order $n \sim 10^5$, and temperatures approach the $T = 3$ K background. Post-formation exposure to galactic cosmic rays implies a $\tau \sim 100$ Myr age, explaining the kinematics of ‘Oumuamua’s inbound trajectory.

Unified Astronomy Thesaurus concepts: [Interstellar medium \(847\)](#); [Small solar system bodies \(1469\)](#)

1. Introduction

‘Oumuamua (1I/2017 U1) passed within 0.25 au of the Sun prior to its 2017 October 19th discovery by Robert Weryk (Meech et al. 2017) among images from the Panoramic Survey Telescope and Rapid Response System (Pan-STARRS) survey. It was initially detected in the course of routine analysis of nightly images taken by the Pan-STARRS project (Chambers et al. 2016), and following several nights of observation with small telescopes, its extrasolar origin was confirmed, leading to a 2017 October 25th discovery announcement through the Minor Planet Center (MPEC 2017). It was then studied intensively over an $l \sim 0.13$ au segment of its outbound trajectory. The overall geometry of ‘Oumuamua’s encounter with the solar system is shown in Figure 1.

With eccentricity, $e = 1.2$, ‘Oumuamua encountered the solar system with $v_\infty = 26$ km s^{-1} . Its hyperbolic incoming trajectory was consistent with Population I disk kinematics and was remarkably close to the local standard of rest (Mamajek 2017; Bailer-Jones et al. 2018). At periastron, ‘Oumuamua achieved a heliocentric velocity of 88 km s^{-1} . Despite experiencing irradiation levels $I > 20$ kW m^{-2} , deep images of ‘Oumuamua showed no coma (Jewitt et al. 2017; Meech et al. 2017), indicating a paucity of micrometer-sized dust in its vicinity (Belton et al. 2018). Its spectrum, moreover, displayed no absorption features and skewed red. Its absolute magnitude (based on an average computed from its strongly variable light curve) was measured to be $H \sim 22.5$ (Jewitt et al. 2017). If one assumes an albedo $p \sim 0.1$, which is typical for small, icy outer solar system bodies, this implies a size (that is, an effective diameter) of order $d \sim 10^4$ cm.

After ‘Oumuamua’s detection and announcement, a variety of observational campaigns were quickly organized on telescopes worldwide, generating a high-quality composite light curve comprising 818 observations and spanning 29.3 days, as summarized by Belton et al. (2018). Frequency analysis of the

light curve shows a power maximum at $P \sim 4.3$ hr, which was interpreted to be half the spin period of a rotating body.³ ‘Oumuamua’s brightness varied by a factor⁴ of ~ 12 , which was explained by positing an elongated shape experiencing complex, nonprinciple axis rotation (Meech et al. 2017; Drahus et al. 2018; Fraser et al. 2018). Subsequently, a detailed analysis by Mashchenko (2019) that employed full light-curve modeling showed that an oblate 115:111:19 \sim 6:6:1 ellipsoid provides the most likely geometry for the body. The light-curve modeling indicates that a prolate “cigar-like” 342 m \times 42 m \times 42 m (i.e., $a:c:c \sim 8:1:1$) ellipsoid also produces a good fit to the data, but requires special tuning of the motion, and is thereby statistically disfavored. Observations with the Spitzer telescope described in Trilling et al. (2018) detected no infrared emission from ‘Oumuamua and placed stringent limits on molecular CO and CO₂ (although not H₂O) outgassing.

Extant photometry for ‘Oumuamua (including multiple *HST* observations taken through the end of 2017) was compiled and analyzed by Micheli et al. (2018), who determined that its outbound trajectory was strongly inconsistent with motion subject only to solar gravity. Those authors determined that a radially outward acceleration component of functional form $\alpha = 4.92 \times 10^{-4} (r/1 \text{ au})^{-2} \hat{r}$ cm s^{-2} superimposed on the Keplerian acceleration permits a substantially improved fit to the observed trajectory. The required magnitude of the nongravitational acceleration component, $A_{ng} \sim 2.5 \times 10^{-4}$ cm s^{-2} at $r \sim 1.4$ au, where ‘Oumuamua was observed at highest signal-to-noise, is of order 10^{-3} of the solar gravitational acceleration.

Micheli et al. (2018) proposed that directed comet-like outgassing from ‘Oumuamua’s surface (e.g., Marsden et al. 1973) was responsible for the acceleration. A model of this

³ Near-uniform rotation is not required to match the light curve. ‘Oumuamua’s rotational motion can exist near the separatrix of a jet-driven pendulum-like Hamiltonian (Seligman et al. 2019).

⁴ The factor of 12 flux variations was computed by averaging the maxima and minima in all oscillations from the digitized composite data.

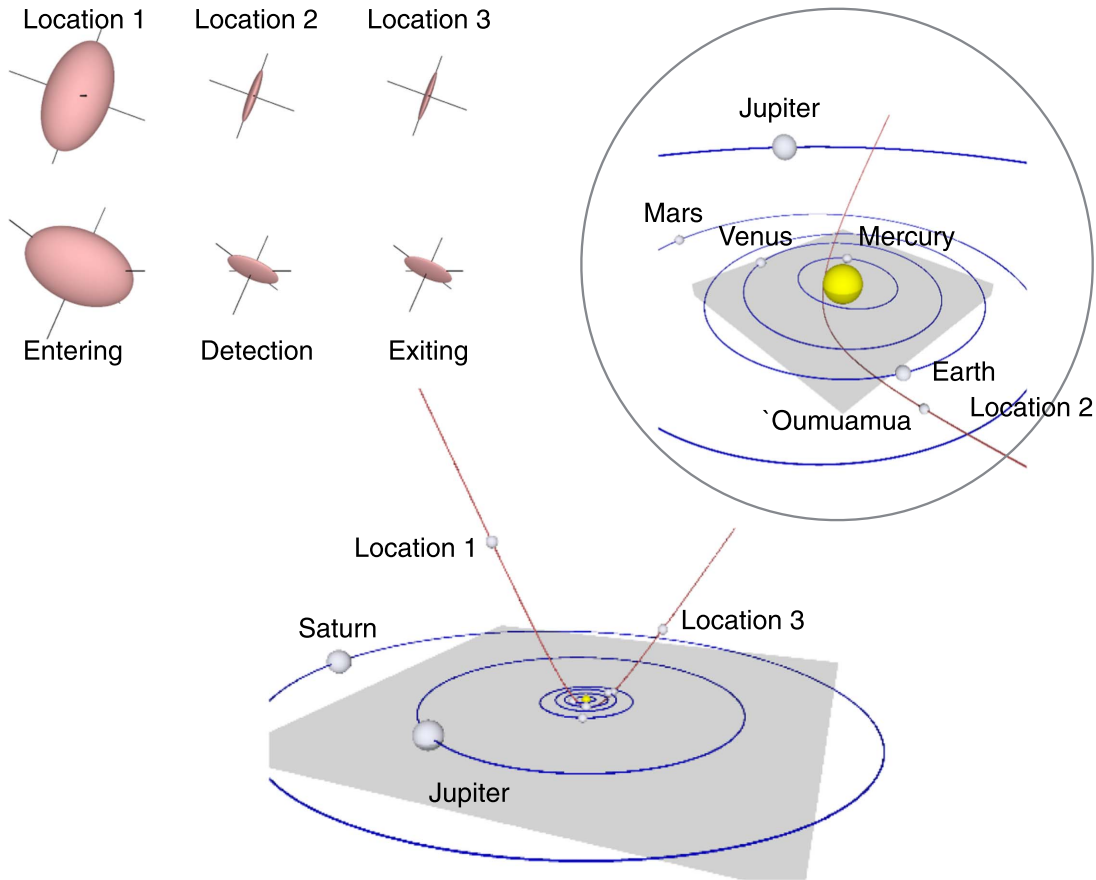


Figure 1. Schematic diagram showing ‘Oumuamua’s size and shape evolution due to H_2 sublimation and its trajectory through the solar system. Pairs of orientations at three discrete points on the trajectory are shown in the upper left.

type requires a mass flux of $\dot{m} \sim 10^4 \text{ g s}^{-1}$ jetting in the solar direction at $v \sim 3 \times 10^4 \text{ cm s}^{-1}$. This acceleration mechanism is seen in solar system comets, and the hypothesis that ‘Oumuamua was a comet-like planetesimal is supported by its featureless red reflection spectrum (Jewitt et al. 2017). It must be stressed, however, that water’s 51 kJ mol^{-1} enthalpy of sublimation ensures that driving the acceleration by vaporizing H_2O ice requires more energy input than ‘Oumuamua received from solar irradiation (Sekanina 2019). We note that ‘Oumuamua’s nongravitational acceleration can also potentially be explained by the action of radiation pressure, but this mechanism requires the bulk density to be extremely low, with $\rho < 10^{-5} \text{ g cm}^{-3}$ (e.g., Bialy & Loeb 2018; Moro-Martín 2019). In short, ‘Oumuamua’s acceleration presents a genuine mystery.

2. Constraints on ‘Oumuamua’s Composition

Because ‘Oumuamua’s orbit was well-determined, the time-dependent flux of solar energy that it received is known to high accuracy. For models that adopt sublimation-driven outgassing as the source of the anomalous acceleration, this energy input $E_{\text{tot}} = 4.5 \times 10^{13} \text{ erg cm}^{-2}$ (integrated over the two years surrounding periastron), must provide both sublimation enthalpy as well as the particle kinetic energy of the outflowing molecules. As was pointed out by Sekanina (2019), this energy budget imparts a strongly nontrivial constraint and indeed, precludes common molecular species as accelerants. In the case of the current consensus view that posits a prolate geometry for

the body and water ice as the substrate, the energy constraint is particularly severe.

To fix ideas, we can first consider an idealized, one-dimensional model in which a face of a rectangular prism of pure, perfectly absorbing ice is illuminated by normally incident sunlight. The flux, \mathcal{N} , of sublimated molecules leaving a directly illuminated patch of surface ice is

$$\mathcal{N} = \frac{(1-p)Q(t) - \epsilon\sigma T_S^4}{\Delta H/N_A + \gamma k T_S}, \quad (1)$$

where $Q(t)$ is the local solar irradiance, ϵ is the surface emissivity, ΔH is the sublimation enthalpy of the ice, T_S is the sublimation temperature, γ is the adiabatic index of the escaping vapor, and p is the surface albedo (assumed to be $p \sim 0.1$ throughout), which is controlled by the admixture of impurities in the sublimating ice.

In the simplest one-dimensional model, a column with unit cross-section, bulk density, ρ , and length, l is exposed at one end to the solar flux. For any given volatile species, one finds the length l , and the associated mass, ρl , accelerated by sublimation that matches the observed acceleration.

For a species with mass μm_u , the sublimating molecules exit isotropically into the hemisphere associated with the zenith normal to the surface. Evaluating the hemispheric integral, the total number of molecules is twice that necessary to produce the anomalous acceleration with a purely normal exiting outflow. The sublimation velocity is $c_s = \sqrt{\gamma k T_S / (\mu m_u)}$ (Probst 1969). The outflow thus produces a change in momentum,

Table 1Surface Covering Fraction, f , Necessary to Power a Jet Consisting of Different Volatile Species

Species	T_{jet} (K)	ρ (g cm $^{-3}$)	ΔH (kJ mol $^{-1}$)	f_{obl}	f_{pro}
H $_2$	6	0.08	1	0.06	0.13
Ne	9	1.5	1.9	0.53	1.21
N $_2$	25	1.02	7.34	0.69	1.58
Ar	30.0	1.75	7.79	0.97	2.20
O $_2$	30.0	1.53	9.26	1.09	2.47
Kr	40.0	3.0	11.53	1.45	3.30
Xe	55.0	3.70	15.79	1.69	3.85
CO $_2$	82.0	1.56	28.84	1.78	4.04
H $_2$ O	155.0	0.82	54.46	2.07	4.72

Note. The enthalpy of sublimation (ΔH), solid density (ρ), and temperature of sublimation (T_{jet}) may be found in Table 3 of Shakeel et al. (2018). We present the surface covering fractions for the best-fit oblate and prolate geometries, denoted by f_{obl} and f_{pro} respectively.

$\mathcal{N}(\mu m_{\text{u}})c_s = \delta m 2|\alpha|$, in the unit column, accelerating net mass, $\delta m = \mathcal{N}(\mu m_{\text{u}} \gamma k T_S)^{1/2} / 2|\alpha|$ in the antisolar direction, \hat{r} . The equivalent length of a column accelerated by a particular species of density ρ is thus given by $l_e \sim \delta m / \rho$. For pure H $_2$ O ice, using the enthalpy of sublimation listed in Table 1, the equivalent length $l_e \sim 15$ m. This dimension is smaller than the shortest axis length $c = 19$ m of Mashchenko’s (2019) best-fit oblate model, thereby ruling out acceleration arising from water ice sublimation. By contrast, the same calculation for H $_2$ ice (which has a sublimation temperature, $T_{\text{H}_2} = 6$ K, sublimation enthalpy $\Delta H = 1$ kJ mol $^{-1}$, and density, ρ_{H_2} g cm $^{-3}$) gives $l_e \sim 540$ m, rendering it a far more viable accelerant.

A more accurate assessment requires that the oblate geometry of ‘Oumuamua be taken explicitly into account. For a given volatile molecule, and a given assumed overall shape, we can calculate the fraction, f , of the total surface area that must be covered by exposed ice. The disk-like $a:a:c \sim 6:6:1$ most-probable model given by Mashchenko (2019) has physical dimensions 115 m \times 111 m \times 19 m. To simplify analytic calculations, we symmetrize this to 113 m \times 113 m \times 19 m. In parallel, we can evaluate the 342 m \times 42 m \times 42 m prolate model.

For these two models, the mass-to-surface-area ratios, η are given by

$$\eta_{\text{obl}} = \frac{2c\rho}{3(1 + (c^2/ea^2)\tanh^{-1}e)}, \quad (2)$$

and

$$\eta_{\text{pro}} = \frac{2a\rho}{3(1 + (a/ec)\sin^{-1}e)}, \quad (3)$$

where $e = \sqrt{1 - c^2/a^2}$ is the ellipsoid’s eccentricity.

Aperiodicity in the light curve suggests that ‘Oumuamua experienced tumbling motion as it traversed the inner solar system. The total amount of energy it received from the solar illumination, therefore, varied in proportion with the instantaneous projected surface area. We define the parameter, ξ , which denotes the average projected surface area of the body divided by its total surface area. When isotropically averaged over all viewing angles, $\xi = 1/4$ for any convex body (Meltzer 1949), but ‘Oumuamua’s tumbling motion prevented it from receiving fully isotropic time-averaged illumination during its observed acceleration.

We use the light curve to infer the amount of flux that ‘Oumuamua received under the assumption of zero solar phase angle and constant surface albedo. With these constraints, the light-curve variations correspond to the instantaneous projected surface area reflecting sunlight directly back to the Earth. We assume that the maxima in the light intensity correspond to the maximal projected surface area. For example, for the oblate spheroidal geometry, this would be a head-on view of the disk. Within these assumptions, the average of the intensity values divided by the maximum intensity gives an estimate of the mean projected surface area as a fraction of the maximum projected surface area.

We introduce the quantity, ζ , which denotes the maximum projected surface area as a fraction of the total surface area. For the oblate and prolate geometries, this quantity is given by,

$$\zeta_{\text{obl}} = \frac{1}{2(1 + (c^2/ea^2)\tanh^{-1}e)}, \quad (4)$$

and

$$\zeta_{\text{pro}} = \frac{a}{2c(1 + (a/ec)\sin^{-1}e)}. \quad (5)$$

We then measure the average maxima of each pulse in the digitized light curve, I_{max} , and the average intensity I_{mean} over all points, and find that $I_{\text{mean}}/I_{\text{max}} \sim 0.42$. This allows us to calculate ξ for both the prolate and oblate geometry, using $\xi = I_{\text{mean}}/I_{\text{max}}\zeta$. Adopting the 6:6:1 and the 8:1:1 shape models and the high signal-to-noise photometry obtained from 2017 October 25 through 2017 November 1 (Belton et al. 2018), we find $\zeta_{\text{oblate}} \sim 0.47$ and $\zeta_{\text{prolate}} \sim 0.32$, corresponding to $\xi_{\text{oblate}} \sim 0.2$ and $\xi_{\text{prolate}} \sim 0.13$.

Combining the above relations gives an expression for the fraction, $f = \eta/(\xi\delta m)$, of an oblate surface that must be covered with sublimating ice to produce the observed radial acceleration,

$$f = \frac{4(\Delta H/N_A + \gamma k T_S)\rho c|\alpha(t)|}{(1-p)Q(t) - e\sigma T_S^4(9\mu m_{\text{u}}\gamma k T_S)^{1/2}\xi\left(1 + \left(\frac{c^2}{ea^2}\right)\tanh^{-1}e\right)}, \quad (6)$$

with an analogous expression holding for the acceleration of a prolate object.

Table 1 lists the covering fractions and other details for a number of species, drawing on the best-fit oblate and prolate models. Sublimating H $_2$ ice can power the jet in both cases. For the oblate geometry, N $_2$, Ne, and Ar are also physically viable, but require high covering fractions. Exposed H $_2$ ice needs to cover only a fraction $0.06(\rho/\rho_{\text{H}_2})$ of the oblate surface to fully account for the motion.

Sublimating H $_2$ ice is difficult to observe. With no prominent emission lines, outgassed H $_2$ would not have registered in the Spitzer Telescope’s 3.6 and 4.5 μm observations (Silvera 1980; Trilling et al. 2018). Moreover, enthalpy-driven cooling associated with the sublimation would have maintained ‘Oumuamua at close to the $T \sim 6$ K sublimation temperature, obviating detection of purely thermal emission.

Given that ‘Oumuamua’s dimensions are known with reasonable confidence, and assuming H $_2$ ice sublimation provided the nongravitational acceleration, the primary remaining unknowns are the bulk density, ρ , and the albedo, p . ‘Oumuamua’s featureless red reflection spectrum is consistent with the coloration of some solar system bodies, with close matches in $B-V$ and $V-R$

colors provided by long-period comet nuclei, Trojan asteroids, and active Jupiter-family comets (Jewitt 2015). A tenable conclusion is that ‘Oumuamua’s coloration is generated by a residuum of presolar grain composition—similar in bulk to the most primitive meteorites—that remained in increasing concentration as the H_2 fraction declined.

3. Evolution of ‘Oumuamua’s Shape

Soon after ‘Oumuamua’s discovery, Domokos et al. (2017) suggested that its unusual shape resulted from abrasion by small particles. The process of isotropized photon-driven sublimation will also produce an evolution that conforms to Domokos et al.’s (2017) theoretical model. Sublimation driven by uniform illumination generates a secular increase in the aspect ratio of the body, with large ratios being reached after a majority of the original mass has been removed.

We have incorporated this phenomenon in a semianalytic model that back-traces ‘Oumuamua’s motion through the solar system and recovers the properties with which it entered the system. We assume that ‘Oumuamua continuously sublimated H_2 at the rate required to generate the observed $\alpha \propto 1/r^2$ nongravitational acceleration, and we assume that ‘Oumuamua’s tumbling motion isotropized exposure of its surface to the Sun over a timescale (\sim days) that is shorter than the timescale over which its received flux varied significantly (\sim weeks). Although the degree of tumbling may not have been sufficient to fully isotropize the exposure, this assumption permits assessment of the density, size, and aspect ratio evolution that ‘Oumuamua experienced while in the vicinity of the Sun.

With our timescale ordering, H_2 gas exits normally from the surface in thin ellipsoidal shells. In each small time increment, the geometry of ‘Oumuamua shifts (approximately) into a new ellipsoid whose axes are each increased or decreased by an amount δh . We simulate this process using time-stepping. We start at the moment of the first observation of ‘Oumuamua in 2017 October, and integrate both forward and backward in time.

Mass loss at each time step is governed by the strength of the nongravitational acceleration. We assume that the best-fit functional form, $\alpha(r)$ is sustained throughout the trajectory. We calculate the change in mass, δm , at each time-step of length Δt , and position in the orbit, r , by invoking the conservation of momentum, where

$$\delta m = \frac{2\alpha(r)\rho_{\text{bulk}}(t)V(t)\Delta t}{\sqrt{\gamma k T_S / (\mu m_u)}}. \quad (7)$$

Here, $V(t)$ and $\rho_{\text{bulk}}(t)$ are the volume and bulk density at each time-step. The resulting differential volume shell, δV , is given by $\delta V = \delta m / \rho_{H_2}$. In order to explicitly demand the conservation of mass and ellipsoidal geometry, we find the root of the cubic equation, $p(\delta h)$ that satisfies,

$$p(\delta h) = \delta V - \frac{4}{3}\pi(a \pm \delta h)(b \pm \delta h)(c \pm \delta h) = 0, \quad (8)$$

where we use the \pm solutions for integrating backwards and forwards in time respectively. Since this differential volume shell is assumed to consist of pure molecular hydrogen, we calculate the resulting bulk density of ‘Oumuamua at each time

step using,

$$\rho_{\text{bulk}}(t \pm \Delta t) = \frac{\rho_{\text{bulk}}(t)V(t) \mp \delta m}{V(t \pm \Delta t)}. \quad (9)$$

We verified that the numerical scheme had converged in timesteps, strictly demanded mass conservation and produced results that were time reversible. This description is, of course, idealized. In reality the outflow may have other molecules as well as dust entrained within it (although the observations do provide strict upper limits). Accounting for constituents other than H_2 would result in a coefficient of order unity in Equation (7).

The evolution of the body in response to the time-varying solar irradiation is displayed in Figure 2. We show simulations that start with bulk densities at the date of detection of $\rho_O = 0.1, 0.3, \text{ and } 0.5 \text{ g cm}^{-3}$. We chart the evolution over a time period of $\tau \sim 3$ months encompassing the most dramatic evolution, but we evolve the simulation for $\tau \sim 2$ yr centered on $t = 0$ corresponding to the periastron passage. The behavior of the aspect ratio, size, and density evolves asymptotically in the regions of the simulation not displayed in the plot. As an example, if ‘Oumuamua had a density of $\rho_O = 0.3 \text{ g cm}^{-3}$ at the time when it was first observed, its dimensions shrank from $\sim 196 \text{ m} \times 196 \text{ m} \times 102$ (with $\rho_{\text{bulk}} \sim 0.093 \text{ g cm}^{-3}$) upon entering the solar system to $\sim 113 \text{ m} \times 113 \text{ m} \times 19 \text{ m}$ when observed to $\sim 110 \text{ m} \times 110 \text{ m} \times 16 \text{ m}$ upon exiting (with $\rho_{\text{bulk}} \sim 0.36 \text{ g cm}^{-3}$). As a consequence of the encounter with the Sun, the total mass dropped by a factor of 5—from 2×10^{11} to $4 \times 10^{10} \text{ g}$. (A visual depiction of this evolution is presented in Figure 1). We conclude that, for a range of plausible initial conditions, ‘Oumuamua entered the solar system with an aspect ratio $\epsilon \sim 2\text{--}3$ and a bulk density $\rho_{\text{bulk}} \sim 0.1 \text{ g cm}^{-3}$.⁵

We can extend the calculation further backward in time to investigate the geometric evolution as ‘Oumuamua traveled through the galaxy and before it encountered the solar system. We perform a similar simulation tracking the aspect ratio, size, and density as it was exposed to the galactic cosmic-ray flux $\Phi_{\text{CR}} \sim 10^9 \text{ ev cm}^{-2} \text{ s}^{-1}$ (White 1996). Using the initial conditions from the preceding calculation for the case where $\rho_O \sim 0.3 \text{ g cm}^{-3}$, we calculate that ‘Oumuamua reached primordial aspect ratios of $\epsilon \sim 1.74, \sim 1.54, \text{ and } \sim 1.28$ after $\tau \sim 10 \text{ Myr}, \sim 30 \text{ Myr}, \text{ and } \sim 100 \text{ Myr}$ of evolution, respectively, with dimensions of $\sim 220 \text{ m} \times 220 \text{ m} \times 130 \text{ m}, \sim 270 \text{ m} \times 270 \text{ m} \times 180 \text{ m}, \text{ and } \sim 440 \text{ m} \times 440 \text{ m} \times 340 \text{ m}$. We also extended the calculation forward in time, and found that if it had not encountered the solar system, ‘Oumuamua would have survived for an additional $\sim 37 \text{ Myr}$ before being reduced to a remnant with bulk density of $\rho_{\text{bulk}} \sim 0.8 \text{ g cm}^{-3}$. In this simple model, prior to encountering the solar system, ‘Oumuamua still had an appreciable fraction of its estimated total lifetime remaining.

4. Formation of Objects Rich in H_2 Ice

H_2 in the gas phase forms via dust-catalyzed reactions and is the dominant constituent of giant molecular clouds (GMCs; Hollenbach & Salpeter 1971; Wakelam et al. 2017). The coldest, highest-density regions within GMCs are prestellar cores, which concentrate along filaments that pervade the overall cloud structure and have $T \leq 10 \text{ K}$ and number

⁵ The script to generate the data in Table 1, these simulations and Figure 2 may be found at https://github.com/DSeligman/Oumuamua_Hydrogen.

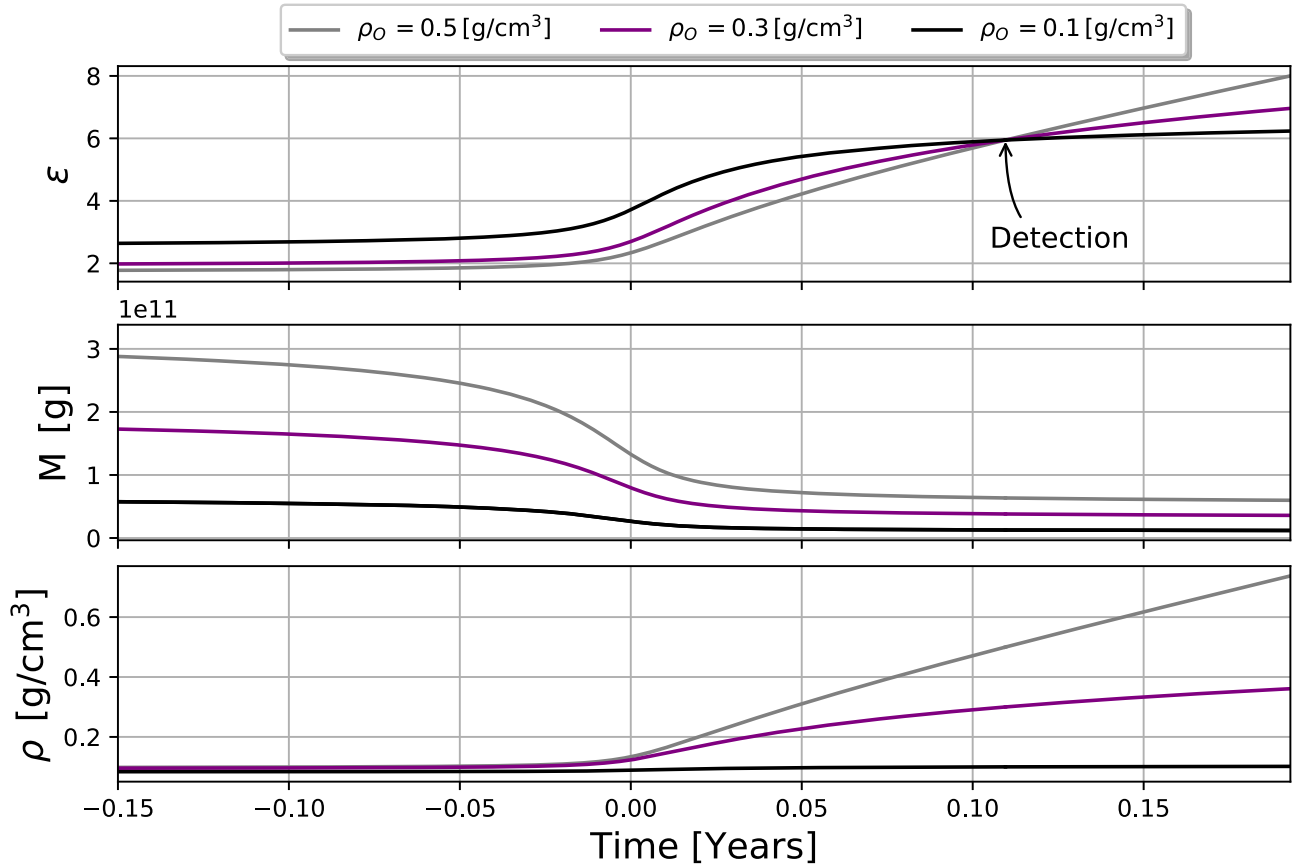


Figure 2. Density, mass, and aspect ratio evolution for ‘Oumuamua as it traveled through the solar system. The periastron passage is displayed at a time, $t = 0$, and the date of detection (Location 2 in Figure 1) is labeled.

densities, $n \geq 10^5 - 10^6 \text{ cm}^{-3}$ (André et al. 2014). At the 2.7 K cosmic background temperature, solid H_2 has a sublimation vapor pressure corresponding to $n \simeq 3 \times 10^5 \text{ cm}^{-3}$ (Anderson 1989). In regions of low cosmic-ray density (such as in the inner regions of M31), CO observations suggest that temperatures very close to the microwave background can be achieved (Loinard & Allen 1998). Recent observations by Kong et al. (2016) of line emission from multiple transitions involving N_2D^+ and N_2H^+ in massive starless/early-stage molecular cloud cores point to excitation temperatures of $T \sim 4 \text{ K}$. Identification of even colder gas may be possible through observation of ortho- H_2D^+ , which has been detected with the Atacama Large Millimeter/submillimeter Array (Friesen et al. 2014). Given a temperature of order 3K in a dense core, nucleated growth of solid hydrogen onto interstellar grains can occur.

Typical interstellar grains, formed from carbon or silicon compounds have sizes, $D_g \sim 1 \mu\text{m}$, cross-sectional areas, $\sigma_g \sim 10^{-8} \text{ cm}^2$, and masses $m_g \sim 10^{-12} \text{ g}$ (Draine 2003). For a dense molecular cloud core with $n_{\text{H}_2} = 10^6 \text{ cm}^{-3}$ and metallicity $Z = 0.01$, this implies a grain number density $n_g = 3 \times 10^{-8} \text{ cm}^{-3}$. Equipartition at $T = 2.7 \text{ K}$ gives a grain velocity $v_g \sim 0.03 \text{ cm s}^{-1}$ (implying a grain-grain collision rate of $\Gamma = n_g \sigma_g v_g = 10^{-17} \text{ s}^{-1}$, which is entirely negligible). For $n_{\text{H}_2} = 10^6 \text{ cm}^{-3}$ and $T = 2.7 \text{ K}$, the sublimation vapor pressure is exceeded by a factor of 3, and molecular hydrogen will freeze out onto the interstellar grains. This process is relatively rapid. The collision rate of H_2 molecules onto grains leads to a grain mass increase rate $dM_g/dt \sim 6 \times 10^{-22} \text{ g s}^{-1}$, and growth timescale $\tau \sim 500 \text{ yr}$ (for sticking probability,

$s = 0.1$). Hence, within several times 10^4 yr of the onset of freeze-out, a significant fraction of the H_2 will sequester onto the small grains.

When condensation conditions for H_2 are achieved, the resulting H_2 -mantled grains in a GMC core are subject to several charging processes, which aid the growth of large dust aggregates in regions where the gas number density is in the range $10^4 \text{ cm}^{-3} < n < 10^6 \text{ cm}^{-3}$ (Ivlev et al. 2015). In short, cold plasma charging tends to give grains negative charge; cosmic rays ionize gas molecules, and electrons, due to their higher velocities, preferentially land on grains. On the other hand, UV radiation stemming from the cosmic-ray ionization events produces photoelectric charging of grains which imparts positive charge to grains. Ivlev et al. (2015) show that competition between the cold-plasma collection and photoemission will create approximately equal abundances of positively and negatively charged dust. Critically, their derived optimum is size-independent, permitting large aggregates to be produced. An H_2 -rich ‘Oumuamua-precursor with $r = 300 \text{ m}$ requires H_2 ice condensates to coagulate within a $D \sim 10^5 \text{ km}$ sided volume of the GMC. If this is to occur over a $\tau \sim 10^4 \text{ yr}$ timescale, characteristic grain velocities of order $v \sim 3 \times 10^{-2} \text{ cm/s}$ are required.

Overall, star formation in GMCs is of order 1% efficient (Shu et al. 1987), with higher efficiencies observed for the densest core regions (Könyves et al. 2015). Macroscopic bodies composed of frozen molecular hydrogen that are not incorporated into stellar systems will be released into low-velocity dispersion galactic orbits, with survival times determined by the ambient cosmic-ray flux. With the back-tracing calculation

described above, we estimate ‘Oumuamua’s initial mass, radius, and age are roughly 3×10^{12} g, 220 m and 10^8 yr, respectively, if its primordial aspect ratio was of order ~ 1.3 , and if its density at the start of observations was $\rho_0 = 0.3 \text{ g cm}^{-3}$.



5. Future Observations

If ‘Oumuamua’s anomalous acceleration stemmed from sublimating H_2 ice, it is likely that a large population of similar objects exists. An analysis by Do et al. (2018) suggests that the space density of ‘Oumuamua-like objects is $n = 0.2 \text{ au}^{-3}$. Our estimate of ‘Oumuamua’s initial mass thus suggests a total mass of $\sim 1 M_\oplus$ of H_2 -rich bodies per star. A galactic sea of unbound planetesimal-sized objects has potential consequences for star and planet formation (Pfalzner & Bannister 2019), and population members will be readily detectable with the forthcoming Large Synoptic Survey Telescope. ESAs proposed Comet Interceptor (Jones & ESA Comet Interceptor Team 2019) mission, moreover, will be well-positioned to provide in situ studies (Seligman & Laughlin 2018).

We thank Fred Adams, Steve Desch, Shuo Kong, and Scott Sandford for useful conversations. This material is based upon work supported by the National Aeronautics and Space Administration through the NASA Astrobiology Institute under Cooperative Agreement Notice NNH13ZDA017C issued through the Science Mission Directorate. We acknowledge support from the NASA Astrobiology Institute through a cooperative agreement between NASA Ames Research Center and Yale University. D.S. acknowledges travel support from the International Space Science Institute (ISSI) ‘Oumuamua Team in Bern, Switzerland.

Note added in proof. Prior to reviewing the proofs, we learned that Füglistaler & Pfenniger (2018) proposed that ‘Oumuamua may have been partially composed of hydrogen ice.

ORCID iDs

Darryl Seligman  <https://orcid.org/0000-0002-0726-6480>
 Gregory Laughlin  <https://orcid.org/0000-0002-3253-2621>

References

- Anderson, H. L. 1989, *A Physicist’s Desk Reference* (Melville, NY: AIP)
- André, P., Di Francesco, J., Ward-Thompson, D., et al. 2014, in *Protostars and Planets VI*, ed. Beuther et al. (Tucson, AZ: Univ. Arizona Press), 27
- Bailer-Jones, C. A. L., Farnocchia, D., Meech, K. J., et al. 2018, *AJ*, **156**, 205
- Belton, M. J. S., Hainaut, O. R., Meech, K. J., et al. 2018, *ApJL*, **856**, L21
- Bialy, S., & Loeb, A. 2018, *ApJL*, **868**, L1
- Chambers, K. C., Magnier, E. A., Metcalfe, N., et al. 2016, arXiv:1612.05560
- Do, A., Tucker, M. A., & Tonry, J. 2018, *ApJL*, **855**, L10
- Domokos, G., Sipos, A. Á, Szabó, G. M., & Várkonyi, P. L. 2017, *RNAAS*, **1**, 50
- Drahus, M., Guzik, P., Waniak, W., et al. 2018, *NatAs*, **2**, 407
- Draine, B. T. 2003, *ARA&A*, **41**, 241
- Fraser, W. C., Pravec, P., Fitzsimmons, A., et al. 2018, *NatAs*, **2**, 383
- Friesen, R. K., Di Francesco, J., Bourke, T. L., et al. 2014, *ApJ*, **797**, 27
- Füglistaler, A., & Pfenniger, D. 2018, *A&A*, **613**, A64
- Hollenbach, D., & Salpeter, E. E. 1971, *ApJ*, **163**, 155
- Ivlev, A. V., Padovani, M., Galli, D., & Caselli, P. 2015, *ApJ*, **812**, 135
- Jewitt, D. 2015, *AJ*, **150**, 201
- Jewitt, D., Luu, J., Rajagopal, J., et al. 2017, *ApJL*, **850**, L36
- Jones, G. & ESA Comet Interceptor Team 2019, Comet Interceptor: A Mission to a Dynamically New Solar System Object. http://www.cometinterceptor.space/uploads/1/2/3/7/123778284/comet_interceptor_executive_summary.pdf
- Kong, S., Tan, J. C., Caselli, P., et al. 2016, *ApJ*, **821**, 94
- Könyves, V., André, P., Men’shchikov, A., et al. 2015, *A&A*, **584**, A91
- Loinard, L., & Allen, R. J. 1998, *ApJ*, **499**, 227
- Mamajek, E. 2017, *RNAAS*, **1**, 21
- Marsden, B. G., Sekanina, Z., & Yeomans, D. K. 1973, *AJ*, **78**, 211
- Mashchenko, S. 2019, *MNRAS*, **489**, 3003
- Meech, K. J., Weryk, R., Micheli, M., et al. 2017, *Natur*, **552**, 378
- Meltzer, B. 1949, *Natur*, **163**, 220
- Micheli, M., Farnocchia, D., Meech, K. J., et al. 2018, *Natur*, **559**, 223
- Moro-Martín, A. 2019, *ApJL*, **872**, L32
- MPEC 2017, IAU Minor Planet Center, U183, <https://minorplanetcenter.net/mpec/K17/K17U11.html>
- Pfalzner, S., & Bannister, M. T. 2019, *ApJL*, **874**, L34
- Probstein, R. 1969, *Problems of Hydrodynamics and Continuum Mechanics* (Philadelphia, PA: SIAM)
- Sekanina, Z. 2019, arXiv:1905.00935
- Seligman, D., & Laughlin, G. 2018, *AJ*, **155**, 217
- Seligman, D., Laughlin, G., & Batygin, K. 2019, *ApJL*, **876**, L26
- Shakeel, H., Wei, H., & Pomeroy, J. M. 2018, *The Journal of Chemical Thermodynamics*, **118**, 127
- Shu, F. H., Adams, F. C., & Lizano, S. 1987, *ARA&A*, **25**, 23
- Silvera, I. F. 1980, *RvMP*, **52**, 393
- Trilling, D. E., Mommert, M., Hora, J. L., et al. 2018, *AJ*, **156**, 261
- Wakelam, V., Bron, E., Cazaux, S., et al. 2017, *MolAs*, **9**, 1
- White, R. S. 1996, *Ap&SS*, **240**, 75